CRYSTAL GROWTH & DESIGN

pubs.acs.org/crystal

Article

Crystallization of a Self-Assembling Nucleator in Poly(L-lactide) Melt

Wei Wang, Angelo Saperdi, Andrea Dodero, Maila Castellano, Alejandro J. Müller, Xia Dong, Dujin Wang, and Dario Cavallo*

Cite This: *Cryst. Growth Des.* 2021, 21, 5880−5888

Read Online

ACCESS | Metrics & More | Article Recommendations | Supporting Information

ABSTRACT: In the present work, crystallization of a soluble nucleator *N*, *N*′, *N*″-tricyclohexyl-1,3,5-benzenetricarboxylamide (TMC-328) in a poly(L-lactic acid) (PLLA) matrix has been studied at different temperatures. Based on the change in solubility with temperature, different levels of supersaturation of TMC-328 in a PLLA matrix can be obtained. This nucleator presents a fibrous structure produced via self-assembling and develops into an interconnected network when the temperature is lowered. The TMC-328 crystal nuclei density is quantified via optical microscopy, using the average distance of the adjacent fibrillar structure, which shows a steady decrease with the decrease in temperature. The crystallization rates of TMC-328 were assessed through rheological measurements of network formation. Both fibrils' density and crystallization kinetics display a power law dependence on supersaturation. For the first time, the solid−melt interfacial energy, the size of the critical nucleus, and the number of molecules making up the critical nucleus of the nucleator TMC-328 in the PLLA matrix have been determined by adopting the classical nucleation theory. The subsequent crystallization of PLLA induced by this nucleator was investigated as a function of the fibrils' spatial density. The crystallization rate of PLLA is enhanced with the increase in the TMC-328 fibrils' density because of the availability of a larger nucleating surface. The self-assembled fibril of TMC-328 can serve as shish to form a hybrid shish-kebab structure after the crystallization of PLLA, regardless of the number of nucleation sites.

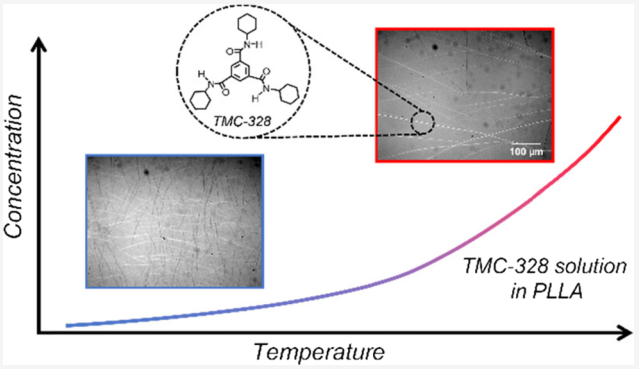

INTRODUCTION

Nucleating agents (NAs) are typically used when crystallization is particularly slow as in the case of poly(ethylene terephthalate) (PET) or to optimize property combinations for specific applications such as for isotactic polypropylene (iPP).[1−5] Apart from the two thermoplastics already mentioned, nucleation additives are mainly relevant for various polyamides (PA-6 and PA-66) and other polyesters such as poly(butylene terephthalate) (PBT) and poly(L-lactic acid) (PLLA). It has been proposed that many materials, such as talc, montmorillonite, carbon nanotubes, and some inorganic powders, have a strong ability to induce nucleation of the abovementioned materials.[6−18] The main problem is the difficulty in dispersing these typically inorganic additives in polymer matrices. Indeed, to act optimally, these NAs need to be dispersed as homogeneously as possible. Obtaining sufficient dispersion is technologically challenging, and to achieve this, a new class of additives that are soluble in molten polymers has been introduced.[19−25]

These soluble NAs are organic, and at high temperatures, they dissolve completely in the polymer melt. During cooling, because of the decrease in solubility, the active molecules undergo phase separation to form networks of fibrils with a high nucleating capacity toward the polymer. The formation of the network is due to the self-organization of the additive molecules that have a lyophilic part capable of solubilizing in the organic liquid (polymeric melt), while the other part is responsible for the establishment of relatively strong bonds (via hydrogen or ionic bonds, usually in a linear fashion), which is necessary for the growth of the microfibrillar structure.[26,27]

As the most concerned eco-friendly thermoplastic polyester, PLLA is increasingly being used in recent years because of its excellent biocompatibility and processability. However, its slow crystallization kinetics caused by the stiffness of the chains and the steric size of the methyl group cannot be neglected any longer.[28−31] This has a strong impact on the processability and final characteristics of the product, limiting the possible practical applications.[31−36] Based on past research, the addition of self-assembly NAs is the most probable effective way to improve the crystallization ability of PLLA. The nucleators,

Received: June 29, 2021
Revised: August 4, 2021
Published: September 1, 2021

Downloaded via UNIV DEL PAIS VASCO on November 17, 2021 at 18:32:38 (UTC).
See https://pubs.acs.org/sharingguidelines for options on how to legitimately share published articles.

ACS Publications

© 2021 The Authors. Published by American Chemical Society

https://doi.org/10.1021/acs.cgd.1c00750
Cryst. Growth Des. 2021, 21, 5880−5888

such as dibenzylidene sorbitol, aliphatic amides, benzenetricarboxylamide derivatives (TMC-328), tetramethylenedicarboxylic dibenzoylhydrazide (TMC-306), and octamethylenedicarboxylic dibenzoylhydrazide (TMC-300), have been utilized not only to enhance the overall crystallization rate but also to tune the crystalline morphology of PLLA.[35−42] For example, Bai et al. found that *N*, *N*′, *N*″-tricyclohexyl-1,3,5-benzenetricarboxylamide (TMC-328) induces fast crystallization and shows noticeable effects on controlling the crystal morphologies of PLLA, including conelike, shish-kebab-like, and needle-like macroscopic structures, because of the high ability in self-organization.[36] Indeed, all studies on PLLA/NA compounds only focus on the crystallization of PLLA after the self-assembling of nucleators and the interaction between them. Nevertheless, until now, the crystallization process of the NA within the PLLA matrix is unrevealed.

In the present work, we wanted to approach the self-organization of TMC-328 molecules in PLLA by comparing this process with the crystallization of organic molecules in solution. This process depends primarily on solubility, which is a function of temperature and concentration. In general, the solubility of a solute is represented by the solubility curve, a diagram showing the concentration as a function of temperature. The solubility curve divides the concentration and temperature range into two distinct zones, one of stability (unsaturated solution) and one of instability (supersaturated solution). Nucleation and growth phenomena depend on supersaturation, that is, the actual solution concentration with respect to the equilibrium one. Thus, the average final size and number of crystals present at the end of the crystallization process will depend on the coordinate of a given system on the solubility plot.[43−45] At a low degree of supersaturation, crystal growth is faster than the nucleation rate, resulting in a larger particle size distribution. However, at a higher degree of supersaturation, crystal nucleation dominates crystallization, eventually resulting in the appearance of smaller crystals.[46,47] This analogy has allowed us to explain the size of the NA network as the concentration and growth temperature are changed. Understanding and controlling the kinetics of the growth of the additive fibrils is crucial for predicting the final morphology of PLLA crystals.

EXPERIMENTAL SECTION

Materials. Samples of PLLA in the pellet form were kindly provided by Purac Biochem (Gorinchem, The Netherlands). The PLLA sample has a weight-average molar mass of 226 kg/mol and a melt flow index of 6.9 g/10 min, and it shows a nominal melting temperature of 175.4 °C. The NA TMC-328 was supplied by the Shanxi Provincial Institute of Chemical Industry (Co., Ltd.), China. The chemical structure is reported in the Supporting Information (Figure S1).

Sample Preparation. Both NAs and PLLA pellets were dried at 50 °C for 24 h before melt-blending in a Brabender mixer. To achieve good dispersion of the NA in PLLA, mixing was performed at 190 °C and 60 rpm for 6 min. Moreover, for the sake of comparison, pure PLLA was also processed using the same method. We investigated the following concentrations of TMC-328 in PLLA: 0.1, 0.2, 0.3, 0.5, and 1 wt %. For simplicity, the samples are abbreviated as PLLA-*x*, where *x* denotes the weight percentage of TMC-328 in the polymer matrix.

Thermogravimetric Analysis. Thermogravimetric analysis (TGA) was performed with a TGA 1 instrument (Mettler Tolendo). About 10 mg of PLLA and TMC-328 samples were used. The material was heated from 20 to 800 °C with a heating rate of 10 °C/min under nitrogen flow. The temperature of the maximum degradation rate for both PLLA and TMC-328 is about 300 °C, as shown in Figure S2 in the Supporting Information.

Polarized Light Optical Microscopy. The crystallization process and crystal morphology of PLLA and TMC-328 were observed in situ using a Leica DMLP optical microscope under crossed polarizers, equipped with a computer-controlled digital camera (Optika B5). The PLLA−TMC 328 films were prepared by compressing the polymer blends on a hot stage at 200 °C. The thermal protocol adopted during experiments was controlled using a Linkam THMS600 hotstage. First, after dissolution at 240 °C for 3 min, a protocol with cooling and further heating at a rate of 5 °C/min was used to determine the point of precipitation and dissolution of the self-assembling structure. Second, in order to study the isothermal crystallization of TMC-328, followed by the nucleation of PLLA on its surface, the samples were cooled to the growth temperature of the network at 10 °C/min from the isotropic melt. Subsequently, the isotherm was maintained for 20 min, and then, the samples were cooled to room temperature at 5 °C/min.

Rheological Analysis. The rheological behavior of all samples was characterized using a rotational shear rheometer (Discovery HR 10, TA Instruments) equipped with a parallel plate (PP) geometry with a diameter of 25 mm and approximately 1 mm gap. The rheometer was equipped with an environmental test chamber (ETC) that uses controlled convection/radiant heating and a constant flow of nitrogen to provide a fast and stable temperature response and prevent polymer degradation. The disk-shaped samples were prepared by compression molding at 200 °C and held at that temperature for 3 min to completely melt PLLA and TMC-328. Time sweep measurements at 175, 180, 185, 190, and 195 °C were performed to monitor the evolution of the storage modulus during the isothermal network formation of TMC-328 after dissolution at 240 °C for 3 min. The applied strain and oscillation frequency were 1% within the linear viscoelastic region (as verified via an amplitude sweep test) and 2 rad/s, respectively.

Differential Scanning Calorimetry. The crystallization behavior of the samples was probed on a TA Instruments DSC 250 under the nitrogen atmosphere. For each measurement, around 5 mg of the sample was placed in a sealed aluminum pan. We applied the same protocol as adopted in the polarized light optical microscopy (POM) test to study the effect of the spatial density of the network on PLLA crystallization.

RESULTS AND DISCUSSION

Crystallization Behavior of TMC-328 in the PLLA Matrix. We first investigated the crystallization and melting behavior of nucleator TMC-328 dispersed in the PLLA matrix. An overview of the POM observation of the PLLA-0.3 sample upon cooling from the homogeneous melt and subsequent heating is shown in Figure 1. When the sample is annealed at 240 °C for 3 min, TMC-328 is dissolved in the PLLA melt, and a homogeneous mixture is obtained above the melting temperature of PLLA because no obvious birefringence of TMC-328 crystals is observed within the resolution scale of POM (Figure 1a). Upon cooling, the nucleator starts to crystallize into a fibrous structure with a length of several tens of micrometers at 175 °C, as indicated by the red arrows shown in Figure 1b. TMC-328 fibrils grow simultaneously from multiple sites in the latter stage of crystallization. In addition to the increase in the fibril length, fibrils also form branches through self-assembling (Figure 1c). Therefore, the resulting network formed by these fibrils is dense because of the connection between the fibrils and the increasing branching number. In the subsequent heating process (Figure 1d−f), the fibrils of TMC-328 formed during cooling crystallization dissolve gradually in the PLLA matrix, which is similar to a solute that dissolves in a solvent.

https://doi.org/10.1021/acs.cgd.1c00750
Cryst. Growth Des. 2021, 21, 5880−5888

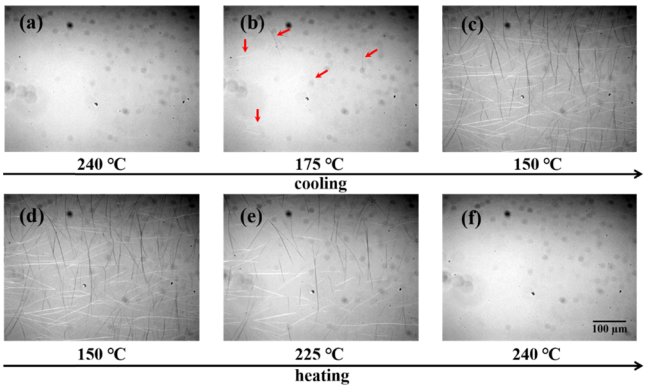

Figure 1. Polarized optical micrographs taken during self-assembling and melting of 0.3% TMC-328 in the PLLA matrix. The contrast of the images has been adjusted to enhance the visibility of the fibrils.

In order to figure out the influence of concentration on the dissolution and self-assembling (crystallization) of TMC-328 in the PLLA matrix, we employed visual observation to judge the appearance and disappearance of crystals during cooling and heating at a rate of 5 °C/min by POM. The corresponding concentration (c)−temperature (T) diagram for dissolution and crystallization of TMC-328 is shown in Figure 2. It is clear

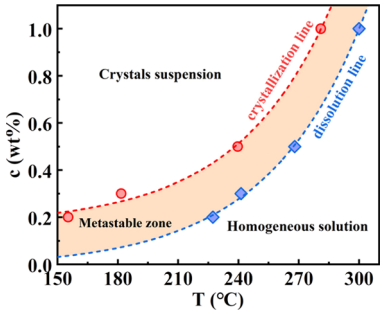

Figure 2. Dissolution and crystallization temperatures of TMC-328 in the PLLA matrix at various concentrations, as determined from POM. The dashed lines are exponential fitting curves.

that the crystallization and the dissolution behaviors of TMC-328 in the PLLA matrix strongly depend on its content. With the increase in the nucleator concentration (0.2−1 wt %), the crystallization temperature of TMC-328 increases from 155 to 281 °C during cooling, and the dissolution temperature increases from 227 to 300 °C, as displayed by the red and blue dashed lines in Figure 2. It should be noted that the blue line in Figure 2 can be regarded as the temperature dependence of the solubility (with equilibrium concentration, c_e) of TMC-328 in the PLLA matrix. The stable solution can be observed in the region below the dissolution line ($c < c_e$), indicating the complete dissolution of TMC-328 in PLLA. Cooling crystallization can occur when the solubility is sufficiently low ($c > c_e$) at a certain temperature, that is, if supersaturation is realized. Between the dissolution line and the crystallization line, the metastable zone (MSZ, orange part) is recognized, in which homogeneous or heterogeneous nucleation occurs and crystals can grow by consuming the supersaturation. When the content of the nucleator is large enough (i.e., in the region above the crystallization line), nucleation is no longer difficult, and the solute rapidly precipitates.

It is well known that the crystallization of semicrystalline polymers largely depends on the self-assembling of the nucleators. Knowing the abovementioned concentration (c)−temperature (T) diagram, the MSZ provides a mean for developing well-controlled crystallization of TMC-328. Therefore, in order to investigate the effect of the self-assembling of TMC-328 on the subsequent crystallization of PLLA, its isothermal crystallization was studied first. We first employed POM to observe the crystal structure of TMC-328 during crystallization at different temperatures selected from the MSZ or at its edges with the crystallization line for the PLLA-0.3 sample (Figure 3). The most intuitive observation from Figure

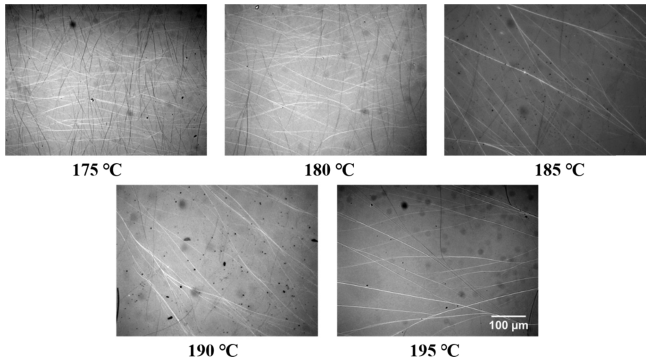

Figure 3. Polarized optical micrographs taken during isothermal crystallization of PLLA-0.3 at the indicated temperatures.

3 is that the higher the temperature, the clearer the fibrous structure is. Indeed, it is because the formation of fewer crystals of TMC-328 at high temperatures results in relatively thicker fibrils. On the other hand, the morphology of tightly packed fibrils of the nucleator is observed during isothermal crystallization at low temperatures, mainly because of the interconnection of many short little fibrils and their branches, displaying the network morphology.

In order to quantify the visual differences in the self-assembling structure formed by TMC-328 during isothermal crystallization in the PLLA matrix at various temperatures, the average distance (d) of the adjacent fibrous crystals was calculated. The distance between the adjacent fibers of TMC-328 is calculated using an image analysis software (Image J), and it is the average of the interfiber distances at 100 randomly selected positions. The choice of this method to quantify the obtained morphology is the only possibility to quantify the obtained morphology, given that the high number of fibrils and their interconnection prevent the direct determination of the fibril concentration. This parameter assumes the physical meaning of the nucleation density or spatial density of the network structure. Figure 4 shows the d value of the adjacent fibrous crystals of TMC-328 in the PLLA-0.3 sample, which increases as the crystallization temperature increases, indicating that the higher the temperature, the lower is the nucleation density.

Having derived morphological information on the self-assembling/crystallization behavior of TMC-328, we now turn our attention to the phase separation kinetics. Rheology can be conveniently applied to follow the crystallization kinetics of TMC-328 in PLLA-0.3, especially because conventional differential scanning calorimetry (DSC) is nonapplicable, as the exceedingly low heat flow is below the sensitivity of the instrument. The evolution of storage modulus, G', with time

https://doi.org/10.1021/acs.cgd.1c00750
Cryst. Growth Des. 2021, 21, 5880−5888

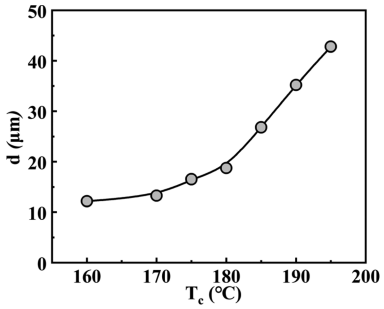

Figure 4. Evolution of the average distance between TMC-328 crystals in PLLA-0.3 as a function of crystallization temperature.

during isothermal crystallization for TMC-328 at different temperatures is shown in Figure 5a. The storage modulus starts from an initial plateau value and then rapidly increases by orders of magnitude with the growing crystallites of TMC-328 in the supersaturated solution, up to a higher plateau value, exhibiting a sigmoidal trend. The differences in the initial plateau modulus are related to the viscosity of the PLLA matrix at different isothermal crystallization temperatures, while the drop in the final plateau modulus with temperature increase is probably attributed to the reduced connectivity of the network structure or to the reduced volume fraction of fibrous crystals (see Figures 3 and 4). The initial storage modulus at 190 and 195 °C are similar, meaning that there is just a minor change in the viscosity in this temperature range. The similarity of storage moduli for the two tested temperatures at 200 s implies a similar structure of the fibrillar network under these conditions. In fact, the relationship between the final modulus and the self-assembling structure of TMC-328 in the PLLA matrix after crystallization is presented in Figure S3. An almost linear increase in the final modulus with the decrease in the average distance between the adjacent fibrils is found.

During isothermal crystallization, amorphous and crystalline phases within rheological measurements can be assumed to behave as two different viscoelastic elements. With the development of crystallization, the storage modulus continues to grow. Therefore, isothermal crystallization kinetics can be analyzed using the following equation:

$$X(t) = \frac{G(t) - G_0}{G_\infty - G_0} \quad (1)$$

where $X(t)$ is the crystallinity (or the degree of transformation), and G_0 and G_∞ are the initial and final storage modulus, respectively. The half-crystallization time, $t_{0.5}$, is defined as the time when the value of $X(t)$ equals 0.5, and it is one of the most intuitive evaluation parameters for crystallization kinetics. Furthermore, a master curve of storage modulus at an arbitrary temperature taken as a reference, extending over a broader time range, was obtained with the software TRIOS. The master curve of storage modulus with crystallization data at 185 °C taken as a reference is shown in Figure 5b, and the corresponding shift factors (f_{shift}) are summarized in the Supporting Information, Table S1. Therefore, the half-crystallization time for the nucleator at a chosen temperature (T^*) can be calculated from the shift factor as follows: $t^*_{0.5}(T^*) = t^{185\ ^\circ C}_{0.5} \times f_{shift\ (T^*)}$.

The half-crystallization time for TMC-328 is plotted as a function of crystallization temperature in Figure 6. A decreasing trend of the crystallization rate with increasing temperature is observed, indicating that in the explored temperature range, the viscosity of the PLLA solvent is not the kinetically controlling factor for crystallization. Therefore, the crystallization kinetics of TMC-328 in this temperature range is dominated by a nucleation process.

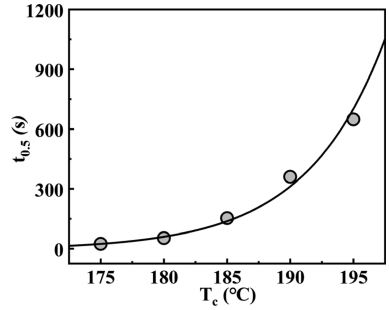

Figure 6. Half-crystallization time as a function of crystallization temperature for TMC-328 in the PLLA-0.3 sample melt.

Relationship between Crystallization and Solubility of TMC-328 in the PLLA Matrix. It is known that the amount of nuclei (N) depends on both time (t) and supersaturation (Δc) for crystallization in a solvent, that is, $N = f(t, \Delta c)$.[48,49] The S-shaped dependence of the number densities of nuclei (i.e., from zero till the maximum number of nuclei) on time at fixed supersaturation has been determined earlier and verified in modern times. On the other hand, supersaturation is also a factor worth noticing because it is the driving force for crystal nucleation.

Indeed, the logistic (sigmoidal) functional description of nucleation kinetics can be used as a general physical rule of the

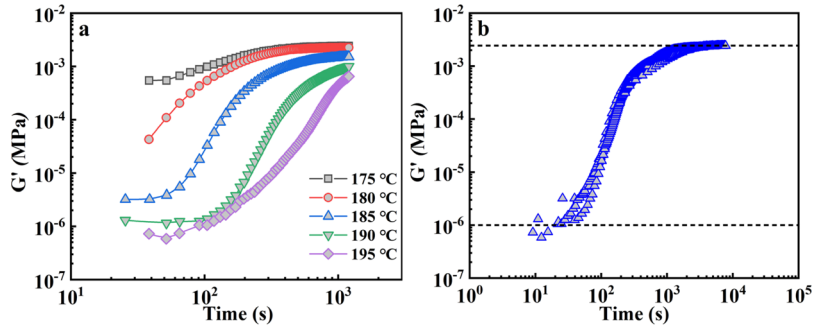

Figure 5. (a) Storage modulus, G', as a function of time for TMC-328 crystallization in PLLA-0.3 samples at different temperatures. (b) Master curve of storage modulus with data at 185 °C taken as a reference, and the initial and final storage moduli are indicated by black dashed lines.

https://doi.org/10.1021/acs.cgd.1c00750
Cryst. Growth Des. 2021, 21, 5880−5888

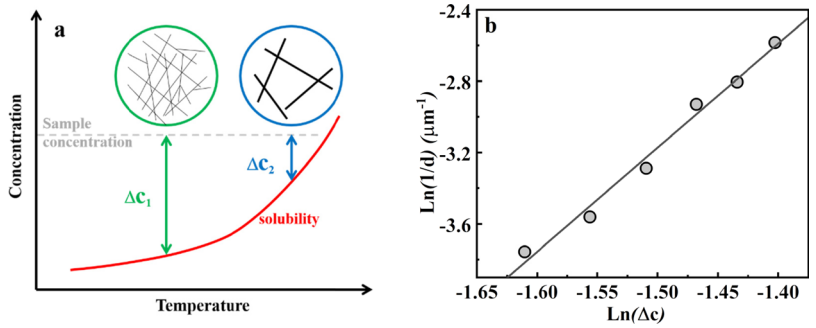

Figure 7. (a) Scheme of the effect of solubility on crystallization at different temperatures. (b) Evolution of number densities of fibrils of TMC-328 as a function of supersaturation at different temperatures.

nucleation process. This is because it just does not only apply to macromolecules and small inorganic molecules but is also valid for classical and two-stage (multistage) nucleation scenarios.[50,51] In this case, a general formula describing the dependence of the nuclei density on time is proposed:

$$\frac{dN}{dt} = kN\left[1 - \frac{1}{1 + \exp[-k(t - t_c)]}\right] \quad (2)$$

where k is the formation frequency of critical nuclei, and t_c is the time of the sigmoid midpoint when N becomes half of the saturation nuclei number density (N_s), i.e., $N = N_s/2$.

To figure out the effect of supersaturation on nucleation kinetics in a solvent, Nývlt has proposed a semiempirical model to express the relationship between the nucleation rate and supersaturation from solutions at a constant cooling speed, which has been widely used:[43]

$$\frac{dN}{dt} = K_n(c - c_e)^n \quad (3)$$

where K_n is the nucleation constant, c and c_e are the actual solution concentration and the solubility, respectively. The exponent n is case-dependent.

Equalizing eqs 2 and 3, we obtain the following equation:

$$N = K_n(c - c_e)^n \frac{1 + \exp(t - t_c)}{k} \quad (4)$$

It is notable that the number of growing crystals and their sizes are interrelated in a reciprocal manner in the process of crystallization. Based on eq 4, it is evident that for obtaining a small number of larger crystals (i.e., slower nucleation), it is necessary to choose a short nucleation time and minimum supersaturation, and vice versa, as indicated in the schematic of Figure 7a, which represents the effect of solubility on the crystallization of TMC-328 at different temperatures within a similar time frame. Because of the formation of extremely thin fibrils, it is hard to judge the crystal size in our work. Therefore, we use the average distance of adjacent crystals, assuming that it is inversely proportional to the crystal size and thus representative of the nuclei number density. From Figure 7a, we can see that with the increase in temperature, supersaturation decreases ($\Delta c_2 < \Delta c_1$) gradually for TMC-328, and then, the corresponding fibrils become larger and sparser (see Figure 3). The quantitative relationship between a parameter proportional to the nuclei number densities ($1/d$) and supersaturation is shown in Figure 7b, confirming that the nucleation density shows a strong dependence on supersaturation.

Figure 8 shows the reciprocal of the half-crystallization time of TMC-328 at different temperatures as determined from

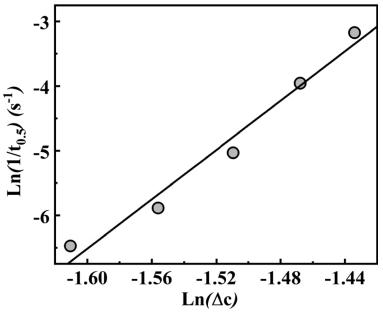

Figure 8. Reciprocal of the half-crystallization time of TMC-328 as a function of supersaturation at different temperatures.

rheology, as a function of supersaturation. Assuming the inverse half-crystallization time as a representative of the nucleation rate, the relationship shown in Figure 8 is in agreement with Nývlt's equation, with an exponent n equal to 19.1. Indeed, as the formation of nuclei is faster, the larger is the driving force for precipitation.

Based on the classical nucleation theory, under the assumption of a spherical nucleus shape, the steady-state nucleation rate (J) in a solvent can be derived as follows:[52,53]

$$J = \frac{dN}{dt} = A\exp\left(-\frac{\Delta G_c}{KT}\right) = A\exp\left(-\frac{16\pi\sigma^3 v_m^2}{3k^3T^3\ln^2 S}\right) \quad (5)$$

where constant A is the pre-exponential factor, ΔG_c is the activation energy of nucleation, K is the Boltzmann constant, σ is the interfacial free energy, ν_m is the solute molecular volume, which can be calculated using the method of atomic and bond contributions of van der Waals volume,[54] T is the crystallization temperature, and S is the supersaturation ratio (concentration c over solubility c_e). Consequently, the critical nuclei size (r^*), critical Gibbs free energy (ΔG^*), and the number of molecules making up the nucleus (n^*) can be determined as follows:[52,55]

$$r^* = \frac{2\nu_m\sigma}{\Delta\mu} \quad (6)$$

$$\Delta G^* = \frac{16\pi\sigma^3 r^{*2}}{3\Delta\mu^2} \quad (7)$$

https://doi.org/10.1021/acs.cgd.1c00750
Cryst. Growth Des. 2021, 21, 5880−5888

$$n^* = \frac{4\pi r^{*3}}{3v_m} \quad (8)$$

where $\Delta\mu$ is the difference in the chemical potential between the solute in the solution and in the crystalline bulk phase, serving as the thermodynamic driving force for nucleation, which is usually estimated by the actual and equilibrium solute mole fraction in the solution, $\Delta\mu \approx kT \ln S = kT \ln \frac{x}{x^*}$.

Usually, the induction time (t_i) is proposed as the t representative of the nucleation rate (J), being inversely proportional to the nucleation rate in the solution of volume V:[56]

$$\ln(t_i) = -\ln JV = -\ln AV + \frac{16\pi\sigma^3 v_m^2}{3k^3T^3 \ln^2 S} \quad (9)$$

For the crystallization of TMC-328 in the PLLA matrix, the overall crystallization kinetics is nucleation-controlled within the temperature range from 175 to 195 °C, as previously discussed. It seems reasonable to assume that the induction time is proportional to the half-crystallization time because in the POM micrograph, a distinct growth of the fibrils is not observed, but rather they appear at once. Therefore, $t_{0.5}$ can be tentatively used as a parameter in eq 9 for the calculation of nucleation kinetics. Figure 9 shows the half-crystallization time

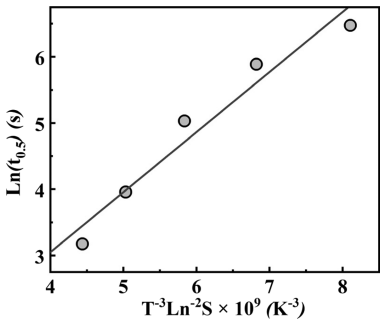

Figure 9. Half-crystallization time of TMC-328 in the PLLA matrix as a function of $T^{-3} \ln^{-2} S$.

of TMC-328 in the PLLA matrix as a function of $T^{-3} \ln^{-2} S$. A linear relationship is observed with a slope of 0.91 and an intercept of 0.58. The interfacial energy σ can be derived from the slope, and then, the corresponding critical parameters can be calculated and are summarized in Table 1.

It is worth noting that an almost twofold change in the free energy barrier for nucleation occurs from a crystallization temperature of 175 to 195 °C, which is associated with an increase in the number of molecules involved in the critical size cluster from 5 to 13.

Table 1. Values of the Supersaturation Ratio, Gibbs Free Energy, the Radius and Number of Molecules in a Critical Nucleus, for TMC-328 Crystallization in the PLLA Matrix at Different Temperatures

T (°C)	S	ΔG^* (kJ/mol)	r^* (nm)	n^*
175	4.87	15.0	0.82	5.1
180	4.31	17.2	0.88	6.3
185	3.80	20.2	0.96	7.9
190	3.37	23.9	1.04	10.2
195	2.99	28.7	1.14	13.4

Crystallization of PLLA Nucleated by TMC-328. For self-assembly systems, the hydrogen bond usually acts as the driving force to build superstructures because of its specificity and directionality.[31,57,58] Based on this point, intensive research has been conducted, also including these self-assembly nucleators that have the acyl group, such as TMC-328, TMC-306, and TMC-300.[18,31,39,59−63] Furthermore, the proton donors (NH) in the acyl group of nucleators are also expected to interact with the proton acceptors (C═O) in PLLA, promoting its crystallization. At the mesoscopic level, it is important to figure out the effect of the network morphology of the nucleator on the crystallization of PLLA.

Figure 10 shows the evolution of the crystallization temperature of PLLA upon cooling from the temperatures

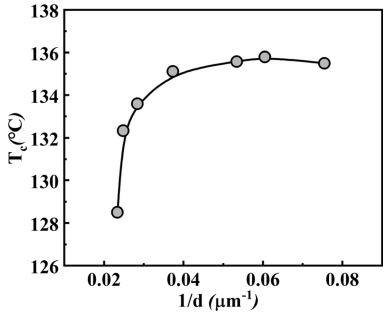

Figure 10. Crystallization temperature of PLLA upon cooling from the isothermal temperatures of TMC-328, as a function of the TMC-328 fibril spatial density in PLLA-0.3.

where TMC-328 isothermally crystallizes as a function of the spatial density of fibrils, that is, their number per unit length ($1/d$) of TMC-328 in the PLLA matrix. When the fibril density becomes lower than about 0.04 μm^{-1}, the crystallization rate of PLLA increases markedly (higher T_c) as the network of fibrous crystals of TMC-328 becomes much denser and structured. Although the size of the crystal structure of TMC-328 is large in the high network formation temperature range (Figure 3), it is not efficient for the subsequent crystallization of PLLA, given the observed lower crystallization temperature of the polymer. Clearly, the crystallization of PLLA is related to the nucleating sites provided by the surface of fibrils of TMC-328. The higher the fibril density, the larger are the nucleating sites. On the other hand, the crystallization rate of PLLA does not change anymore when the nuclei density exceeds 0.04 μm^{-1} at network formation temperatures of TMC-328 below 185 °C. There may be various reasons to explain this observation. The crystallization temperature under nonisothermal conditions is influenced by both nucleation and growth processes. Therefore, even if there are many nucleation sites provided by the fibrillar structure of TMC-328 after isothermal crystallization at temperatures below 185 °C, the continuous growth of PLLA crystals becomes the rate-determining step because of the early-stage collision of extremely close crystals formed on the surface of dense fibrils. Another speculative explanation might refer to the "consumption" of hydrogen bond sites because of the strong intermolecular association within the self-assembling nucleator at lower temperatures. In fact, the intensity of the hydrogen bond for a given system generally increases with decreasing temperature because the enthalpy of bond formation is usually negative.[31]

To further understand the effect of TMC-328 on PLLA crystallization, the crystal morphologies of PLLA under the

https://doi.org/10.1021/acs.cgd.1c00750
Cryst. Growth Des. 2021, 21, 5880−5888

presence of various networks of the nucleator were characterized by polarized light microscopy, as shown in Figure 11. It has been shown that TMC-328 is randomly

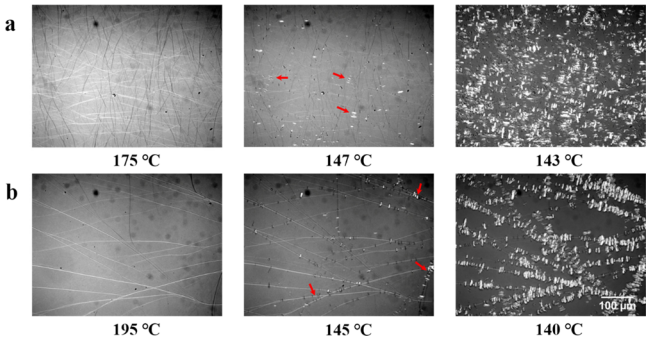

Figure 11. Polarized optical micrographs taken during cooling after self-assembling of TMC-328 at (a) 175 °C and (b) 195 °C for 20 min in PLLA-0.3.

distributed in the form of an interconnected network structure formed by fibrils at low temperatures and of an isolated fibril structure at high temperatures in the PLLA melt (Figure 3). For both cases, disk-shaped kebabs of PLLA grow on the surface of the self-organized TMC-328 structures and form shish-kebab-like structures, which are indicated by the red arrows, and this result is in agreement with the previous studies.[35,36] The final morphology of PLLA is similar after TMC-328 self-assembling at both temperatures (i.e., 175 and 195 °C, see Figure 11), notwithstanding the difference in the TMC-328 fibril spatial density. Several mechanisms have been proposed to explain the crystallization of PLLA with the aid of TMC-328, which include the epitaxial growth proposed by Bai et al.,[36] and hydrogen bonding interactions proposed by Xie et al.[63] This latter mechanism suggests that the absorbed PLLA chains onto the surface of self-organized fibrils of TMC-328 will form the primary nuclei, driven by hydrogen bonding interactions, and then, the outer layer molecules will crystallize on the surface of the primary nuclei when the temperature is further decreased. The interpretation has the support of Fourier-transform infrared (FT-IR) data, while the idea of epitaxial growth is still lacking direct evidence so far.

CONCLUSIONS

The present work focuses on the isothermal crystallization of TMC-328 at different temperatures in a molten PLLA matrix and on the subsequent induced crystallization of PLLA. This nucleator presents a fibrous structure produced via self-assembling and develops into an interconnected network when its crystallization temperature is decreased. The crystal nuclei density of TMC-328 is quantified by means of the average distance (d) between adjacent fibrils, showing a steady decrease with the decrease in temperature. On the basis of the classical nucleation theory, the solid−melt interfacial energy, the size of the critical nucleus, and the number of molecules making up the critical nucleus of TMC-328 have been determined in the PLLA matrix for the first time, using the half-crystallization time obtained from rheological measurements.

The crystallization rate of PLLA is first largely enhanced with the increase in the TMC-328 fibril density because of the availability of a large nucleating surface. The acceleration then reaches a plateau with a further increase in the fibril spatial density because of the growth stage becoming the rate-determining step. Notwithstanding the nucleation density of the nucleator, the morphology after the crystallization of PLLA is the hybrid shish-kebab structure, which is in agreement with previous studies.

ASSOCIATED CONTENT

Supporting Information

The Supporting Information is available free of charge at https://pubs.acs.org/doi/10.1021/acs.cgd.1c00750.

Chemical structure of the NA; TGA scans for PLLA and TMC-328; final storage modulus of PLLA-0.3 as a function of the reciprocal of the average distance ($1/d$) of the adjacent TMC-328 fibrils; and the shift factor of storage modulus versus time curves at different temperatures (PDF)

AUTHOR INFORMATION

Corresponding Author

Dario Cavallo − *Department of Chemistry and Industrial Chemistry, University of Genoa, Genova 16146, Italy;* orcid.org/0000-0002-3274-7067; Email: dario.cavallo@unige.it

Authors

Wei Wang − *Department of Chemistry and Industrial Chemistry, University of Genoa, Genova 16146, Italy;* orcid.org/0000-0001-7299-3564

Angelo Saperdi − *Department of Chemistry and Industrial Chemistry, University of Genoa, Genova 16146, Italy*

Andrea Dodero − *Department of Chemistry and Industrial Chemistry, University of Genoa, Genova 16146, Italy*

Maila Castellano − *Department of Chemistry and Industrial Chemistry, University of Genoa, Genova 16146, Italy;* orcid.org/0000-0002-0930-7522

Alejandro J. Müller − *POLYMAT and Department of Polymers and Advanced Materials: Physics, Chemistry and Technology, Faculty of Chemistry, University of the Basque Country UPV/EHU, 20018 Donostia—San Sebastian, Spain; IKERBASQUE, Basque Foundation for Science, Bilbao 48009, Spain;* orcid.org/0000-0001-7009-7715

Xia Dong − *Beijing National Laboratory for Molecular Sciences, Institute of Chemistry, Chinese Academy of Sciences, Beijing 100190, China; University of Chinese Academy of Sciences, Beijing 100049, China;* orcid.org/0000-0002-6409-7011

Dujin Wang − *Beijing National Laboratory for Molecular Sciences, Institute of Chemistry, Chinese Academy of Sciences, Beijing 100190, China; University of Chinese Academy of Sciences, Beijing 100049, China;* orcid.org/0000-0002-2063-0873

Complete contact information is available at: https://pubs.acs.org/10.1021/acs.cgd.1c00750

Notes

The authors declare no competing financial interest.

ACKNOWLEDGMENTS

W.W. thanks the China Scholarship Council (CSC) for funding his Ph.D. scholarship. We would like to thank the financial support provided by the BIODEST project; this project has received funding from the European Union's

Horizon 2020 research and innovation program under the Marie Sklodowska-Curie grant agreement no. 778092.

REFERENCES

(1) Chen, Y.; Xu, M.; Li, Y.; He, J. Effects of nucleating, agent and nucleation promoter on the crystallization of polyethylene terephthalate. *Acta Polym. Sin.* **1999**, *1*, 7−14.
(2) Jiang, X. L.; Luo, S. J.; Sun, K.; Chen, X. D. Effect of nucleating agents on crystallization kinetics of PET. *Express Polym. Lett.* **2007**, *1*, 245−251.
(3) Beck, H. Heterogeneous nucleating agents for polypropylene crystallization. *J. Appl. Polym. Sci.* **1967**, *11*, 673−685.
(4) Zhao, S.; Cai, Z.; Xin, Z. A highly active novel β-nucleating agent for isotactic polypropylene. *Polymer* **2008**, *49*, 2745−2754.
(5) Feng, Y.; Jin, X.; Hay, J. N. Effect of nucleating agent addition on crystallization of isotactic polypropylene. *J. Appl. Polym. Sci.* **1998**, *69*, 2089−2095.
(6) Şanlı, S.; Durmus, A.; Ercan, N. Effect of nucleating agent on the nonisothermal crystallization kinetics of glass fiber- and mineral-filled polyamide-6 composites. *J. Appl. Polym. Sci.* **2012**, *125*, E268−E281.
(7) Li, J.; Fang, Z.; Zhu, Y.; Tong, L.; Gu, A.; Liu, F. Isothermal crystallization kinetics and melting behavior of multiwalled carbon nanotubes/polyamide-6 composites. *J. Appl. Polym. Sci.* **2007**, *105*, 3531−3542.
(8) Won, J. C.; Fulchiron, R.; Douillard, A.; Chabert, B.; Varlet, J.; Chomier, D. The crystallization kinetics of polyamide 66 in non-isothermal and isothermal conditions: Effect of nucleating agent and pressure. *Polym. Eng. Sci.* **2000**, *40*, 2058−2071.
(9) Zhang, L.; Hong, Y.; Zhang, T.; Li, C. Nonisothermal Crystallization Behaviors of Poly(butylene terephthalate) Nucleated with Elastomer-Modified Nano-SiO2, a Commercial Nucleating Agent (P250), and Talc. *J. Macromol. Sci. B* **2010**, *49*, 514−527.
(10) Richter, F.; Schmidt, H. W. Supramolecular Nucleating Agents for Poly(butylene terephthalate) Based on 1,3,5-Benzenetrisamides. *Macromol. Mater. Eng.* **2013**, *298*, 190−200.
(11) Qin, Y.; Yang, J.; Yuan, M.; Xue, J.; Chao, J.; Wu, Y.; Yuan, M. Mechanical, barrier, and thermal properties of poly(lactic acid)/poly(trimethylene carbonate)/talc composite films. *J. Appl. Polym. Sci.* **2014**, *131*, 6855−6866.
(12) Yan, S.; Yin, J.; Yang, Y.; Dai, Z.; Ma, J.; Chen, X. Surface-grafted silica linked with l-lactic acid oligomer: A novel nanofiller to improve the performance of biodegradable poly(l-lactide). *Polymer* **2007**, *48*, 1688−1694.
(13) Monticelli, O.; Bocchini, S.; Gardella, L.; Cavallo, D.; Cebe, P.; Germelli, G. Impact of synthetic talc on PLLA electrospun fibers. *Eur. Polym. J.* **2013**, *49*, 2572−2583.
(14) Li, X.; Yin, J.; Yu, Z.; Yan, S.; Lu, X.; Wang, Y.; Cao, B.; Chen, X. Isothermal crystallization behavior of poly(L-lactic acid)/organo-montmorillonite nanocomposites. *Polym. Compos.* **2009**, *30*, 1338−1344.
(15) Wang, S.; Han, C.; Bian, J.; Han, L.; Wang, X.; Dong, L. Morphology, crystallization and enzymatic hydrolysis of poly(L-lactide) nucleated using layered metal phosphonates. *Polym. Int.* **2011**, *60*, 284−295.
(16) Fujisawa, S.; Saito, T.; Kimura, S.; Iwata, T.; Isogai, A. Comparison of mechanical reinforcement effects of surface-modified cellulose nanofibrils and carbon nanotubes in PLLA composites. *Compos. Sci. Technol.* **2014**, *90*, 96−101.
(17) Xing, Q.; Zhang, X.; Dong, X.; Liu, G.; Wang, D. Low-molecular weight aliphatic amides as nucleating agents for poly (L-lactic acid): Conformation variation induced crystallization enhancement. *Polymer* **2012**, *53*, 2306−2314.
(18) Xing, Q.; Li, R.; Dong, X.; Luo, F.; Kuang, X.; Wang, D.; Zhang, L. Enhanced Crystallization Rate of Poly(l-lactide) Mediated by a Hydrazide Compound: Nucleating Mechanism Study. *Macromol. Chem. Phys.* **2015**, *216*, 1134−1145.
(19) Kristiansen, M.; Werner, M.; Tervoort, T.; Smith, P.; Blomenhofer, M.; Schmidt, H.-W. The Binary System Isotactic Polypropylene/Bis(3,4-dimethylbenzylidene)sorbitol: Phase Behavior, Nucleation, and Optical Properties. *Macromolecules* **2003**, *36*, 5150−5156.
(20) Shepard, T. A.; Delsorbo, C. R.; Louth, R. M.; Walborn, J. L.; Norman, D. A.; Harvey, N. G.; Spontak, R. J. Self-organization and polyolefin nucleation efficacy of 1,3:2,4-di-p-methylbenzylidene sorbitol. *J. Polym. Sci., Part B: Polym. Phys.* **1997**, *35*, 2617−2628.
(21) Thierry, A.; Straupe, C.; Lotz, B.; Wittmann, J. Physical gelation: a path towards ideal dispersion of additives in polymers. *Polym. Commun. (Guildford)* **1990**, *31*, 299−301.
(22) Ke, N. Z. N. Effect of DMDBS on crystallization behavior of polypropylene. *China Plast.* **2008**, *7*, 78−82.
(23) Sreenivas, K.; Basargekar, R.; Kumaraswamy, G. Phase separation of DMDBS from PP: effect of polymer molecular weight and tacticity. *Macromolecules* **2011**, *44*, 2358−2364.
(24) Wang, B.; Utzeri, R.; Castellano, M.; Stagnaro, P.; Müller, A. J.; Cavallo, D. Heterogeneous nucleation and self-nucleation of isotactic polypropylene microdroplets in immiscible blends: from nucleation to growth-dominated crystallization. *Macromolecules* **2020**, *53*, 5980−5991.
(25) Menyhárd, A.; Gahleitner, M.; Varga, J.; Bernreitner, K.; Jäskeläinen, P.; Øysæd, H.; Pukánszky, B. The influence of nucleus density on optical properties in nucleated isotactic polypropylene. *Eur. Polym. J.* **2009**, *45*, 3138−3148.
(26) Ma, P.; Deshmukh, Y. S.; Wilsens, C. H.; Ryan Hansen, M.; Graf, R.; Rastogi, S. Self-assembling process of Oxalamide compounds and their nucleation efficiency in bio-degradable Poly-(hydroxyalkanoate)s. *Sci. Rep.* **2015**, *5*, 1−9.
(27) Shen, T.; Xu, Y.; Cai, X.; Ma, P.; Dong, W.; Chen, M. Enhanced crystallization kinetics of poly(lactide) with oxalamide compounds as nucleators: effect of spacer length between the oxalamide moieties. *RSC Adv.* **2016**, *6*, 48365−48374.
(28) Blomqvist, J. RIS Metropolis Monte Carlo studies of poly(l-lactic), poly(l,d-lactic) and polyglycolic acids. *Polymer* **2001**, *42*, 3515−3521.
(29) Hoffman, J. D.; Davis, G. T.; Lauritzen, J. I. The rate of crystallization of linear polymers with chain folding. In *Treatise on solid state chemistry*. Springer: 1976, pp. 497−614.
(30) Hoffman, J. D.; Miller, R. L.; Marand, H.; Roitman, D. B. Relationship between the lateral surface free energy .sigma. and the chain structure of melt-crystallized polymers. *Macromolecules* **1992**, *25*, 2221−2229.
(31) Li, C.; Luo, S.; Wang, J.; Wu, H.; Guo, S.; Zhang, X. Conformational regulation and crystalline manipulation of PLLA through a self-assembly nucleator. *Biomacromolecules* **2017**, *18*, 1440−1448.
(32) Ma, P.; Jiang, L.; Xu, P.; Dong, W.; Chen, M.; Lemstra, P. J. Rapid Stereocomplexation between Enantiomeric Comb-Shaped Cellulose-g-poly(l-lactide) Nanohybrids and Poly(d-lactide) from the Melt. *Biomacromolecules* **2015**, *16*, 3723−3729.
(33) Pal, A. K.; Katiyar, V. Nanoamphiphilic Chitosan Dispersed Poly(lactic acid) Bionanocomposite Films with Improved Thermal, Mechanical, and Gas Barrier Properties. *Biomacromolecules* **2016**, *17*, 2603−2618.
(34) Kakroodi, A. R.; Kazemi, Y.; Ding, W.; Ameli, A.; Park, C. B. Poly(lactic acid)-Based in Situ Microfibrillar Composites with Enhanced Crystallization Kinetics, Mechanical Properties, Rheological Behavior, and Foaming Ability. *Biomacromolecules* **2015**, *16*, 3925−3935.
(35) Bai, H.; Huang, C.; Xiu, H.; Zhang, Q.; Deng, H.; Wang, K.; Chen, F.; Fu, Q. Significantly improving oxygen barrier properties of polylactide via constructing parallel-aligned shish-kebab-like crystals with well-interlocked boundaries. *Biomacromolecules* **2014**, *15*, 1507−1514.
(36) Bai, H.; Zhang, W.; Deng, H.; Zhang, Q.; Fu, Q. Control of Crystal Morphology in Poly(l-lactide) by Adding Nucleating Agent. *Macromolecules* **2011**, *44*, 1233−1237.
(37) Lai, W.-C. Thermal Behavior and Crystal Structure of Poly(l-lactic acid) with 1,3:2,4-Dibenzylidene-d-sorbitol. *J. Phys. Chem. B* **2011**, *115*, 11029−11037.

https://doi.org/10.1021/acs.cgd.1c00750
Cryst. Growth Des. 2021, 21, 5880−5888

(38) Nakajima, H.; Takahashi, M.; Kimura, Y. Induced Crystallization of PLLA in the Presence of 1,3,5-Benzenetricarboxylamide Derivatives as Nucleators: Preparation of Haze-Free Crystalline PLLA Materials. *Macromol. Mater. Eng.* **2010**, *295*, 460−468.
(39) Bai, H.; Huang, C.; Xiu, H.; Zhang, Q.; Fu, Q. Enhancing mechanical performance of polylactide by tailoring crystal morphology and lamellae orientation with the aid of nucleating agent. *Polymer* **2014**, *55*, 6924−6934.
(40) Cai, Y.; Yan, S.; Fan, Y.; Yu, Z.; Chen, X.; Yin, J. The nucleation effect of N,N′-bis(benzoyl) alkyl diacid dihydrazides on crystallization of biodegradable poly(l-lactic acid). *Iran. Polym. J.* **2012**, *21*, 435−444.
(41) Lai, W.-C.; Liao, J.-P. Nucleation and crystal growth kinetics of poly(l-lactic acid) with self-assembled DBS nanofibrils. *Mater. Chem. Phys.* **2013**, *139*, 161−168.
(42) Xing, Q.; Li, R.; Zhang, X.; Dong, X.; Wang, D.; Zhang, L. Tailoring crystallization behavior of poly (L-lactide) with a low molecular weight aliphatic amide. *Colloid Polym. Sci.* **2015**, *293*, 3573−3583.
(43) Nývlt, J. Kinetics of nucleation in solutions. *J. Cryst. Growth* **1968**, *3-4*, 377−383.
(44) Grove, C., Jr; Jelinek, R. V.; Schoen, H. M. Crystallization from solution. In *Advances in Chemical Engineering*. Elsevier: 1962, pp. 1−60.
(45) Boistelle, R.; Astier, J. P. Crystallization mechanisms in solution. *J. Cryst. Growth* **1988**, *90*, 14−30.
(46) Nanev, C. N. Relationship between number and sizes of crystals growing in batch crystallization: Nuclei number density, nucleation kinetics and crystal polydispersity. *J. Cryst. Growth* **2020**, *546*, No. 125786.
(47) Yang, H.; ter Horst, J. H.; Crystal nucleation of small organic molecules. In *New perspectives on mineral nucleation and growth*. Springer, 2017, pp. 317−337, DOI: 10.1007/978-3-319-45669-0_16.
(48) Nanev, C. N.; Hodzhaoglu, F. V.; Dimitrov, I. L. Kinetics of insulin crystal nucleation, energy barrier, and nucleus size. *Cryst. Growth Des.* **2011**, *11*, 196−202.
(49) Sauter, A.; Roosen-Runge, F.; Zhang, F.; Lotze, G.; Jacobs, R. M. J.; Schreiber, F. Real-time observation of nonclassical protein crystallization kinetics. *J. Am. Chem. Soc.* **2015**, *137*, 1485−1491.
(50) Nanev, C. N.; Tonchev, V. D. Sigmoid kinetics of protein crystal nucleation. *J. Cryst. Growth* **2015**, *427*, 48−53.
(51) Nanev, C. N. Advancements (and challenges) in the study of protein crystal nucleation and growth; thermodynamic and kinetic explanations and comparison with small-molecule crystallization. *Prog. Cryst. Growth Charact. Mater.* **2020**, *66*, No. 100484.
(52) Yang, H.; Svärd, M.; Zeglinski, J.; Rasmuson, Å. C. Influence of solvent and solid-state structure on nucleation of parabens. *Cryst. Growth Des.* **2014**, *14*, 3890−3902.
(53) Yang, H.; Rasmuson, Å. C. Nucleation of butyl paraben in different solvents. *Cryst. Growth Des.* **2013**, *13*, 4226−4238.
(54) Zhao, Y. H.; Abraham, M. H.; Zissimos, A. M. Fast calculation of van der Waals volume as a sum of atomic and bond contributions and its application to drug compounds. *J. Organ. Chem.* **2003**, *68*, 7368−7373.
(55) Kashchiev, D. *Nucleation*. Elsevier: 2000.
(56) Kashchiev, D.; van Rosmalen, G. M. Review: Nucleation in solutions revisited. *Cryst. Res. Technol.* **2003**, *38*, 555−574.
(57) Xue, C.; Jin, S.; Weng, X.; Ge, J. J.; Shen, Z.; Shen, H.; Graham, M. J.; Jeong, K.-U.; Huang, H.; Zhang, D.; Guo, M.; Harris, F. W.; Cheng, S. Z. D.; Li, C. Y.; Zhu, L. Self-assembled "supra-molecular" structures via hydrogen bonding and aromatic/aliphatic microphase separation on different length scales in symmetric-tapered bisamides. *Chem. Mater.* **2004**, *16*, 1014−1025.
(58) Lawrence, D. S.; Jiang, T.; Levett, M. Self-assembling supramolecular complexes. *Chem. Rev.* **1995**, *95*, 2229−2260.
(59) Fan, Y.; Zhu, J.; Yan, S.; Chen, X.; Yin, J. Nucleating effect and crystal morphology controlling based on binary phase behavior between organic nucleating agent and poly(l-lactic acid). *Polymer* **2015**, *67*, 63−71.
(60) Zhang, H.; Bai, H.; Liu, Z.; Zhang, Q.; Fu, Q. Toward High-Performance Poly(l-lactide) Fibers via Tailoring Crystallization with the Aid of Fibrillar Nucleating Agent. *ACS Sustainable Chem. Eng.* **2016**, *4*, 3939−3947.
(61) Kawamoto, N.; Sakai, A.; Horikoshi, T.; Urushihara, T.; Tobita, E. Physical and mechanical properties of poly(L-lactic acid) nucleated by dibenzoylhydrazide compound. *J. Appl. Polym. Sci.* **2007**, *103*, 244−250.
(62) Li, C.; Dou, Q.; Bai, Z.; Lu, Q. Non-isothermal crystallization behaviors and spherulitic morphology of poly(lactic acid) nucleated by a novel nucleating agent. *J. Therm. Anal. Calorim.* **2015**, *122*, 407−417.
(63) Xie, Q.; Han, L.; Shan, G.; Bao, Y.; Pan, P. Polymorphic Crystalline Structure and Crystal Morphology of Enantiomeric Poly(lactic acid) Blends Tailored by a Self-Assemblable Aryl Amide Nucleator. *ACS Sustainable Chem. Eng.* **2016**, *4*, 2680−2688.

https://doi.org/10.1021/acs.cgd.1c00750
Cryst. Growth Des. 2021, 21, 5880−5888